Amphiphilic nanoparticle delivery enhances the anticancer efficacy of a TLR7 ligand via local immune activation

Inès Mottas[a,b,1], Ahmet Bekdemir[c,1], Alessandra Cereghetti[a], Lorenzo Spagnuolo[a,b], Yu-Sang Sabrina Yang[d,e], Marie Müller[c], Darrell J. Irvine[e,f,g,h,d], Francesco Stellacci[c,i,1], Carole Bourquin[a,b,j,*,1]

[a] Ecole de Pharmacie Genève-Lausanne (EPGL), University of Lausanne, University of Geneva, Switzerland
[b] University of Fribourg, Chair of Pharmacology, Fribourg, Switzerland
[c] Institute of Materials, EPFL, Lausanne, Switzerland
[d] Dept. of Materials Science and Engineering, Massachusetts Institute of Technology, Cambridge, MA 02139, USA
[e] Koch Institute for Integrative Cancer Research, Massachusetts Institute of Technology, Cambridge, MA 02139, USA
[f] The Ragon Institute of Massachusetts General Hospital, Massachusetts Institute of Technology and Harvard University, Cambridge, MA 02139, USA
[g] Department of Biological Engineering, Massachusetts Institute of Technology, Cambridge, MA 02139, USA
[h] Howard Hughes Medical Institute, Chevy Chase, MD 20815, USA
[i] Interfaculty Bioengineering Institute, EPFL, Lausanne, Switzerland
[j] Department of Anesthetics, Pharmacology and Intensive Care, Faculty of Medicine, University of Geneva, Switzerland

ARTICLE INFO

Keywords:
Nanoparticles
Drug delivery
Cancer immunotherapy
Lymph nodes
TLR7 agonist

ABSTRACT

Although immunotherapy shows great promise for the long-term control of cancer, many tumors still fail to respond to treatment. To improve the outcome, the delivery of immunostimulants to the lymph nodes draining the tumor, where the antitumor immune response is initiated, is key. Efforts to use nanoparticles as carriers for cancer immunotherapy have generally required targeting agents and chemical modification of the drug, and have unfortunately resulted in low delivery and therapeutic efficiency. Here, we report on the efficacy of gold nanoparticles with approximately 5 nm hydrodynamic diameter coated with a mixture of 1-octanethiol and 11-mercaptoundecanesulfonic acid for the delivery of an immunostimulatory TLR7 ligand to tumor-draining lymph nodes. The drug was loaded without modification through nonspecific adsorption into the ligand shell of the nanoparticles, taking advantage of their amphiphilic nature. After loading, nanoparticles retained their stability in solution without significant premature release of the drug, and the drug cargo was immunologically active. Upon subcutaneous injection into tumor-bearing mice, the drug-loaded particles were rapidly transported to the tumor-draining lymph nodes. There, they induced a local immune activation and fostered a cytotoxic T-cell response that was specific for the tumor. Importantly, the particle-delivered TLR7 ligand blocked the growth of large established tumors and significantly prolonged survival compared to the free form of the drug. Thus, we demonstrate for the first time that nanoparticle delivery of a TLR7 immunostimulant to the tumor-draining lymph nodes enhances antitumor immunity and improves the outcome of cancer immunotherapy.

1. Introduction

Cancer immunotherapy aims to activate the body's own defenses in order to control or even cure the disease. To date, this treatment strategy can lead to long-term survival in up to 50% of patients with advanced cancer [1]. A major challenge that limits the efficacy of immunotherapy is the lack of efficient delivery of immunostimulants to the tumor-draining lymph nodes, where antitumor immunity is initiated. Indeed, the tumor-draining lymph nodes contain high levels of dendritic cells that are maintained in an immature and therefore non-functional state by the tumor [2]. Strategies such as the intranodal injection of immunostimulants have confirmed that the direct re-activation of lymph node-resident dendritic cells promotes the development of strong cytotoxic T-cell responses which are essential for anticancer immunity [3,4]. Injection into non-superficial lymph nodes is however a technically challenging procedure that requires highly

* Corresponding author. Section of Pharmaceutical Sciences, University of Geneva, Rue Michel-Servet 1, 1211, Geneva, Switzerland.
E-mail address: carole.bourquin@unige.ch (C. Bourquin).
[1] IM and AB contributed equally to this work (first authors). FS and CB contributed equally to this work (senior authors).

specific expertise and equipment. Nanoparticle delivery systems represent an interesting alternative, as they can promote drug transport into tumor-draining lymph nodes following subcutaneous injection and at the same time limit dissemination of the drug into the systemic circulation [5,6]. At present, targeting immunostimulatory drugs to the lymph nodes in order to restore dendritic cell function is an unmet need in cancer immunotherapy [7].

There have been a number of reports on the use of nanoparticles to aid cancer immunotherapy through delivery of immunomodulatory molecules [8]. Typical design in these approaches includes chemical conjugation of nanoparticles to drug molecules which entails their structural modification [9]. Moreover, additional targeting agents can be attached for selective accumulation of drug-nanoparticle conjugates into tumor-draining lymph nodes or interaction with dendritic cells [8]. However, targeted delivery via conjugation of specific molecules to nanoparticles is debated, as it leads to low delivery efficiency [10]. We have reported that gold nanoparticles (~5 nm in diameter) coated with an approximate 2:1 mixture of 1-octanethiol (OT) and 11-mercaptoundecanesulfonic acid (MUS) could be loaded with hydrophobic drugs in the ligand shell without any chemical modification to the drug [11,12]. The amphiphilic nature of the ligand shell that has a hydrophobic core (the OT ligand and the alkyl part of the MUS ligand) allows hydrophobic molecules to spontaneously partition into the ligand shell from a water/acetone mixture, upon acetone evaporation. This approach that non-specifically adsorbs drugs in the inner part of the ligand shell was developed in the literature for other particles and recently proven for ours [13]. Furthermore, these particles have been shown to reach lymph nodes efficiently when subcutaneously injected [12]. The combination of these two properties, together with the very low toxicity of these particles, make them ideal candidates for drug delivery in the case of cancer immunotherapy. Given that the amphiphilic nature of these particles is key for their drug loading, these particles will hereafter be referred to as amphiphilic nanoparticles (AmpNP).

Small molecule Toll-like receptor (TLR) 7 agonists are potent immunostimulants for dendritic cells used in topical application for the treatment of skin malignancies [14,15]. Their systemic application for non-skin cancers, although effective in preclinical models [16,17], has not been successful in patients due to a disbalance between safety and efficacy [18,19]. Here we used AmpNP to deliver the small molecule TLR7 agonist resiquimod (R848) to tumor-draining lymph nodes in order to foster a local immune response at the site where the antitumor response is initiated. Our results show that AmpNP carrying R848 improved the antitumor efficacy of the drug in tumor-bearing mice. Compared to the same dose of free R848, treatment with AmpNP-R848 conjugate considerably increased the survival of mice, highlighting the therapeutic potential of these nanoparticles *in vivo*.

2. Material and methods

2.1. Materials for AmpNP synthesis

1-octanethiol (> 97%) (OT), gold(III) chloride trihydrate (> 99.9%), sodium borohydride (99%), chloro(triphenylphosphine) gold(I), borane tert-butylamine complex (BtBA) (97%) and resiquimod (R848, > 98%) were purchased from Sigma Aldrich and used without further purification. 11-mercaptoundecane sulfonate sodium salt (MUS) was synthesized according to a previously reported protocol [20]. All solvents were ACS grade and used without further purification.

2.2. Synthesis and characterization of AmpNP

MUS (0.3 mmol in 20 ml methanol) and OT (0.15 mmol in 20 ml methanol) were mixed in a vial and added to gold (III) salt solution (0.45 mmol $HAuCl_4$ in 75 ml ethanol) at room temperature. Sodium borohydride (300 mg in 75 ml ethanol) was added dropwise to the previous mixture at room temperature over the course of 1 h. The reaction was left stirring for 3 h before placing at 4 °C overnight. The precipitated product was washed several times with methanol by centrifugation (5000 g). The product was then dissolved in 20 ml water and washed with deionized water through Amicon® Ultra-15 centrifugal filter devices (30'000 Da MWCO). Finally, it was freeze-dried and stored as powder for further use.

TEM characterization was carried out as follows: A drop of 0.1 mg/ml AmpNP solution was loaded on a carbon-coated copper grid (CF300-Cu Square Mesh TedPella) and air dried. Images were acquired with a FEI Tecnai Spirit 130 kV electron microscope. Image analysis was done with ImageJ software.

For hydrodynamic diameter analysis, 1000 µl of AmpNP solution at 0.1 mg/ml in PBS buffer was filtered through 0.22 µm PTFE syringe filters (Whatman®) was measured with a dynamic light scattering instrument (Malvern ZetaSizer) at room temperature for 10 measurements averaged from a total of 3 datasets. Zeta potential measurements were carried out in PBS before and after conjugation of R848 to AmpNPs. The NP solutions were filtered through 0.22 µm PTFE syringe filters (Whatman®) prior to each measurement. After loading into semi disposable zeta-potential cuvettes provided by Malvern, at least 10 data points were acquired for each measurement (results were averaged by at least n = 3).

2.3. R848 loading onto nanoparticles

In a 20 ml glass vial, 1 mg of R848 was dissolved in 5 ml acetone and added to AmpNP solution (10 mg in 5 ml H_2O). The mixture was stirred overnight to allow evaporation of acetone, thus enforcing R848 to partition into the nanoparticles' hydrophobic surface ligands. The solution was filtered through 0.45 µm polyethersulfone filters and washed with deionized water through Amicon® Ultra-15 centrifugal devices (30'000 Da MWCO) until no detectable R848 was found in filtrate (checked with absorption spectroscopy). The final AmpNP-R848 solution was diluted into 1 ml H_2O and stored at 4 °C for further use.

To calculate the number of R848 molecules per nanoparticle, 10 µl of AmpNP-R848 stock solution (10 mg AmpNP-R848 in 1 ml deionized water) was mixed into 0.9 ml of ethanol. 100 µl of KCN solution (10 mg/ml in methanol) was added to the previous solution and vortexed for 2 min. The colored solution turned colorless and was centrifuged at 5'000 g for 30 s to remove precipitates. The supernatant was measured with absorbance spectroscopy at 327 nm for quantification of R848. The amount of AmpNP in solution was calculated by assuming an approximate molecular weight of 120'000 Da based on the previously reported method [21]. The encapsulation efficiency was found to be around 30% which was determined by adding 0.1 mg R848 into 10 mg AmpNP. In order to ensure complete loading, we added an excess of R848 (around 1 mg) in the AmpNP solution throughout most of the experiments.

2.4. BODIPY 650/665-X labelling of AmpNP

6-(((4,4-Difluoro-5-(2-thienyl)-4-bora-3a,4a-diaza-s-indacene-3-yl) styryloxy)acetyl)- aminohexanoic acid, succinimidyl ester (BODIPY 650/665-X, SE, Life Technologies) was thiolated through the succinimidyl ester group to yield BODIPY-SH. A stock solution of BODIPY-SH dye in acetone was used to place exchange by mixing 50-fold molar excess of BODIPY to AmpNP solution in water over 2 days. Acetone was then added to the reaction mixture (5:1 vol ratio of acetone:reaction volume) and centrifuged in 13'000 rcf with table-top centrifuge. Free dye was washed out with additional acetone-centrifugation cycles. Finally, the remaining pellet was dried under vacuum, dissolved in 1 ml water and used as 10 mg/ml fluorescently labelled AmpNP stock solution [22].

2.5. AmpNP-R848 stability in biological media

To assess the colloidal stability of AmpNP-R848 during storage, the stock solution of AmpNP-R848 (10 mg AmpNP-R848/ml) was diluted 1:50 in PBS, complete cell culture medium, 10% serum or 100% fetal bovine serum prior to incubation at 37 °C for 24 h. The absorbance spectrum was measured from 400 to 700 nm with a resolution of 2 nm using a microplate reader (Clariostar from BMGlabetech). Optical density (O.D.) at 400 nm was set as 1. To assess the release of R848 over time, stock solution of R848-AmpNP was incubated in PBS or 100% human serum at 37 °C. The solution was then filtered through a centrifugal dialysis membrane (Amicon 3'000 MWCO, 10'000 g centrifugation) for 15 min and assessed by absorbance spectroscopy.

2.6. AmpNP uptake by immune cells

J774.1 macrophages (ATCC) were plated at 5×10^4 cells/well in a chambered coverglass (Lab-tek II from Nunc) with 3 μg/ml of BODIPY 650/665-labelled AmpNP in DMEM high glucose without phenol red (Gibco) supplemented with 10% fetal calf serum (FCS, Gibco) and 1 mg/ml ciprofloxacin (Bayer). After 3 h, LysoTracker Blue DND-22 (Invitrogen) diluted 1:1'000 was added for an additional hour to stain acidic cell compartments before live cell imaging by confocal microscopy (Zeiss 710) at 20× and 63× magnification.

2.7. Dendritic cell viability and maturation phenotype after AmpNP exposure

Bone marrow-derived dendritic cells (BMDC) were generated as previously described [23], plated at 5×10^4 cells/well in a flat-bottom 96-well plate (Corning) in RPMI 1640 (Gibco), 10% fetal calf serum (FCS) (Gibco) and 1% penicillin/streptomycin (PAA laboratories) and exposed to increasing concentrations of AmpNP-R848. After 24 h exposure, BMDC were harvested for flow cytometry analysis and the supernatant was stored at −20 °C for later ELISA quantification of mouse interleukin 6 (IL-6) and TNFα (ELISA Max Deluxe, Biolegend) according to the manufacturer's protocol. At 3 μg AmpNP/ml, the highest concentration used, AmpNP neither interfered with ELISA nor with flow cytometry readings according to a previously described test protocol [24].

For flow cytometry analysis, dendritic cells were stained with Zombie fixable viability dye (1:100; Biolegend) for 30 min in PBS. Cells were then incubated with unlabeled anti-CD16/32 (1:100) to block Fc receptors (Biolegend) for 10 min at 4 °C before addition of the following antibodies: APC-CD80 (16-10.A1), FITC-MHC-II (d,b) (M5/114.15.2) and APC-Cy7-CD11c (N418) (all from Biolegend). Samples were acquired with a MACSquant analyzer (Miltenyi Biotec) or a Novocyte flow cytometer (ACEA Biosciences). Data were analyzed using FlowJo 10.0.8r1.

2.8. AmpNP-R848 injection into mice

Female C57BL/6JRj or Balb/c (Janvier or Charles River) were housed under specific pathogen-free conditions and used at 6–15 weeks of age. Animal experimentation was conducted according to Swiss or U.S. regulations. Unless stated otherwise, 110 μg of AmpNP-R848 (total dose: 6 μg R848) in 100 μl PBS were injected subcutaneously in the right hind limb of mice after 4% isoflurane (Piramal Healthcare) anesthesia.

2.9. AmpNP biodistribution in mice

To assess the biodistribution of AmpNP-R848 in lymph nodes and spleen following s.c. injection, the following procedure was followed: Lymph nodes draining the s.c. injection site, as confirmed with the use of Patent blue V (Sigma-Aldrich), and contralateral lymph nodes were isolated 24 h post-injection. Imaging of lymph nodes was performed with a Leica M125 stereomicroscoscope at 10× magnification. Alternatively, lymph nodes and spleen were solubilized using 200 μl 25% wt tetramethylammonium hydroxide (TMAH; Sigma-Aldrich). The samples were dissolved in freshly prepared Aqua Regia to dissolve the gold nanoparticles shaking for two days at RT. Prior to ICP-MS quantification of gold atoms on an HPLC ICP-MS PERKIN ELMER ELAN DRCII the samples were diluted with MilliQ water. To assess the biodistribution of AmpNP in a panel of lymphoid and non-lymphoid organs at different time points following subcutaneous and intravenous injection, the following procedure was followed: C57Bl/6 mice (n = 3/group) received 300 μg of AmpNP resuspended in 100 μl PBS via tail vein i.v. injection or s.c. Tissue samples (lung, kidney, liver, bladder, inguinal lymph nodes, 1 ml of blood) were collected 4 or 24 h post injection, and weights were recorded. Samples were dissolved in 1 ml freshly prepared aqua regia for three days. The mixture solutions were then diluted in 2% nitric acid to bring up the total volume per sample to 3 ml. Samples were centrifuged for 15 min at 3000 rpm at 4 °C immediately prior to ICP-OES analysis on a Horiba Activa.

2.10. Assessment of immune activation in lymph nodes

To obtain single cell suspensions, lymph nodes were cut with a scalpel, shaken for 10–20 min at 37 °C in RPMI 1640 (Gibco) supplemented with 2 mM $CaCl_2$ (Acros Organics), 3 mg/ml collagenase and 13.3 mg/ml DNAse I (both from Worthington).

RNA was isolated from lymph node cells with the RNeasy Plus Mini kit (Qiagen) according to manufacturer's protocol. RNA was converted to cDNA using Maxima H Minus First strand cDNA Synthesis Kit (ThermoFisher) with a Biometra T3000 Thermocycler (Labrepco). Real-time PCR amplification was performed with the KAPA SYBR fast qPCR kit (Kapa Biosystems) on a Step One Plus instrument (ThermoFisher). Primers (Eurogentech) were designed as follows: ifn-α (5′-gtgaccttcctcagactca-3′,3′-tccaaagtccttcctgtcct-5′), tnf-α (5′-aaatggcctccctctcat-3′, 3′-cctccaccttggtggtttg-5′), hprt(5′-atgagcgcaagttgaatctg-3′,3′-cagatggccacaggactaga-5′).

2.11. Serum cytokine quantification

The mouse inflammation panel from LegendPlex (Biolegend) was used according to the manufacturer's protocol. This predefined panel allows simultaneous quantification of 13 mouse cytokines including IL-1α, IL-1β, IL-6, IL-10, IL-12p70, IL-17A, IL-23, IL-27, CCL2, INF-γ, TNF-α and GM-CSF. Samples were acquired by Novocyte and analyzed using FlowJo software.

2.12. Impact of AmpNP-R8 on tumor growth in mice

The CT26 colon carcinoma cell line (ATCC) was cultured in RPMI 1640 (Gibco), 10% FCS (Life Technologies), 1% penicillin/streptomycin, 1% sodium pyruvate, 10 mM HEPES buffer, and 50 mM β-mercaptoethanol (all from PAA laboratories) before subcutaneous injection in the right flank of Balb/c mice (2.5×10^5 cells in 100 μl PBS). When the tumors reached a mean volume of 200 mm^3 ($\pi/3$*length*width^2), mice were treated 5 times at 3-day intervals with 6 μg of R848 loaded on AmpNP. In accordance with the 3R principles, mice were sacrificed upon reaching the following stop criteria: tumor volume exceeding 3000 mm^3, necrosis zone of the tumor exceeding 25 mm^2 or a decrease in body weight greater than 10%. These events were used for the survival curve.

To assess immune cell activation, mice were sacrificed the day after the last R848 injection for spleen isolation. A single cell suspension were obtained by passing the spleens through a 40 μm cell strainer (Corning Inc.) using a plunger before erylysis (Pharm lyse from BD Bioscience). For flow cytometry analysis, cells were stained with the same protocol as for dendritic cells using the following Abs: PerCP-CD3

(145-2C11), APC-Cy7-CD8 (53-6.7), BV510-CD69 (H1.2F3), FITC-PD1 (HA2-7B1) (all from Biolegend). Tetramer staining was performed with PE-H-2Ld MuLV gp70 tetramers (MBL international corporation) prior to antibody staining according to manufacturer's protocol.

2.13. Statistical analysis

Statistical analysis was performed with GraphPad Prism 6.0e software. Significance between two groups was evaluated with unpaired two-tailed Student's T-test. Significance of multiple groups in comparison to control group was evaluated using one-way ANOVA followed by Dunnett's multiple comparison test. Repeated-measure two-way ANOVA followed by Dunnett's multiple comparison test was used to evaluate statistical difference in tumor growth, while log rank test was used to evaluate statistical difference in the survival curve. Asterisks (*,$P \leq 0.05$; **,$p \leq 0.01$; ***,$p \leq 0.001$; ****, $p \leq 0.001$) indicate significant differences.

3. Results

3.1. Design of AmpNP and R848 loading

AmpNP were synthesized by a simple reduction of water-soluble gold salt with a borane-based reducing agent in the presence of thiolated ligands. A stoichiometric mixture of hydrophilic 11-mercaptoundecane sulfonate (MUS) and hydrophobic 1-octanethiol (OT) was introduced in the reaction solution in order to stabilize nanoparticles after the nucleation and growth (Fig. 1A). The resulting gold nanoparticles were found to be highly monodispersed, having 2.2 nm in core diameter (Supplementary Fig. 1) and approximately 5 nm in total hydrodynamic diameter (Fig. 1B). The detailed characterization of AmpNP can be found in Supplementary Fig. 1. The surface of AmpNP has two prominent characteristics: (i) An inner ligand shell which is composed of alkane chains that forms a template to sequester hydrophobic drugs and (ii) highly charged terminal sulfonate groups which provide long term colloidal stability in biological buffers. Consequently, the loading of R848 in the hydrophobic pockets required only an additional incubation step followed by washing the free molecules out of the solution *via* dialysis. It is worth highlighting the ease of preparing AmpNP-R848 in our protocol as it does not entail any additional chemical functionalization, which is generally a prerequisite for covalent attachment methodologies [25]. Subsequent quantification experiments with absorbance spectroscopy revealed the average number of R848 to be 12 molecules per nanoparticle. In addition, these absorbance measurements demonstrated that R848 molecules remained structurally intact during their stay in hydrophobic pockets of AmpNP and did not undergo any chemical modifications (Supplementary Fig. 2A). AmpNPs retained their highly charged structure and were colloidally stable after R848 loading as suggested by zeta-potential measurements (Fig. 1C).

After loading the drug molecules onto AmpNP, we investigated whether there was a premature drug release at physiological conditions. To this end, R848-loaded AmpNP were incubated in PBS or 100% serum at 37 °C for several hours and release kinetics were measured with absorbance spectroscopy. Our results demonstrated that a maximum of 10% of the R848 load detached from the AmpNP within 24 h (Fig. 1D). We reasoned that this initial release of R848 molecules could be due to imperfect fitting of drug molecules within the hydrophobic pockets of AmpNP due to crowding of R848. Nevertheless, even after 48 h approximately 85% of R848 remained associated with AmpNP independently of the biological buffer used for the experiment. Additional release experiments in 2-(N-morpholino)ethanesulfonic acid (MES) buffer at pH 5.5 demonstrated that a substantial amount of R848 is released into the solution possibly due to protonation of amine groups and hence rendering the molecule water-soluble.

Aggregation or premature degradation of drug delivery systems represents a major challenge that limits the use of nanoparticles for biomedical applications [26]. To evaluate the colloidal stability of AmpNP, we measured their absorbance spectrum, which reflects the size and shape of the gold core [27], after incubation in various biological conditions that could affect their colloidal stability [28]. We show that the AmpNP-R848 remained stable after a 6-month storage at 4 °C, as well as after 24 h at 37 °C in different biological media (Supplementary Fig. 2B). Similar results were obtained for AmpNP without R848 cargo (data not shown). Our results confirmed the colloidal stability of AmpNP-R848 during storage and in biological conditions.

3.2. In vitro immunoactivity of R848 cargo in AmpNP

Nanoparticles are readily taken up in the organism by phagocytic cells of the immune system such as macrophages and dendritic cells [29]. These cells are responsible for the initiation of immune responses, and thus represent a prime target for immunostimulatory drugs such as R848. In addition, since R848 is a synthetic ligand of the endosomal receptor TLR7, delivery to the endosome of phagocytic cells is essential for its immunological activity [30]. We incubated fluorescently labelled AmpNP with the J774.1 macrophage cell line for 4 h and observed endosomal accumulation (Supplementary Fig. 3A). To verify that AmpNP-R848 were not toxic for immune cells, bone marrow-derived dendritic cells (BMDC) were exposed to increasing concentrations of R848 or AmpNP-R848 for 24 h. Both R848 and AmpNP-R848 enhanced cell survival, as previously shown [31]. R848-loaded AmpNP did not affect cell viability when compared to free R848 up to a concentration of 14 μg/ml AmpNP, which corresponds to 0.5 μg/ml R848 (Supplementary Fig. 3B).

In order to determine whether R848 delivered by AmpNP remained immunologically active, we measured pro-inflammatory cytokines in the supernatants of BMDC 24 h after exposure to AmpNP-R848. The following factors serve as indicators for TLR7 activation of dendritic cells: (i) secretion of proinflammatory cytokines such as IL-6, TNF-α, IL-12, and IFN-α and β; (ii) upregulation of antigen-presenting and costimulatory molecules such as MHC-II and CD80 [16,32]. In our experiments, AmpNP-R848 clearly induced the secretion of the cytokines IL-6 and TNFα in a dose-dependent manner (Supplementary Fig. 3C). Additionally, BMDC exposed to AmpNP-R848 expressed higher surface levels of the maturation markers MHC-II and CD80, which are essential for effective T-cell priming (Supplementary Fig. 3D) [33,34]. The induction of proinflammatory cytokines and maturation markers was similar for AmpNP-R848 and the equivalent amount of free R848, indicating that R848 delivered by AmpNP did not lose immunological activity.

Importantly, the AmpNP without cargo did not induce cytokine secretion nor dendritic cell maturation (Supplementary Figs. 3C and 3D), demonstrating that AmpNP alone were not immune-activating and suggesting that the AmpNP preparations were free from immunostimulatory contaminants.

3.3. Lymph node accumulation and in vivo immune activation by AmpNP-R848

To assess the biodistribution of AmpNP-R848, we isolated the inguinal and axillary lymph nodes of mice 24 h after subcutaneous injection of the particles into the inguinal area (Fig. 2A). The inguinal area is known to be drained by the inguinal lymph nodes, that in turn drain to the axillary lymph nodes [35]. The stereomicroscope picture clearly showed that AmpNP accumulated in the first draining lymph node (ipsilateral inguinal node) and second draining lymph node (ipsilateral axillary node) after 24 h (Fig. 2C). In contrast, contralateral lymph nodes appeared particle-free. To quantify the accumulation of AmpNP, the gold content in the different lymph nodes was determined by inductively coupled plasma mass spectrometry (ICP-MS). Gold ions were detected almost exclusively in the ipsilateral draining lymph

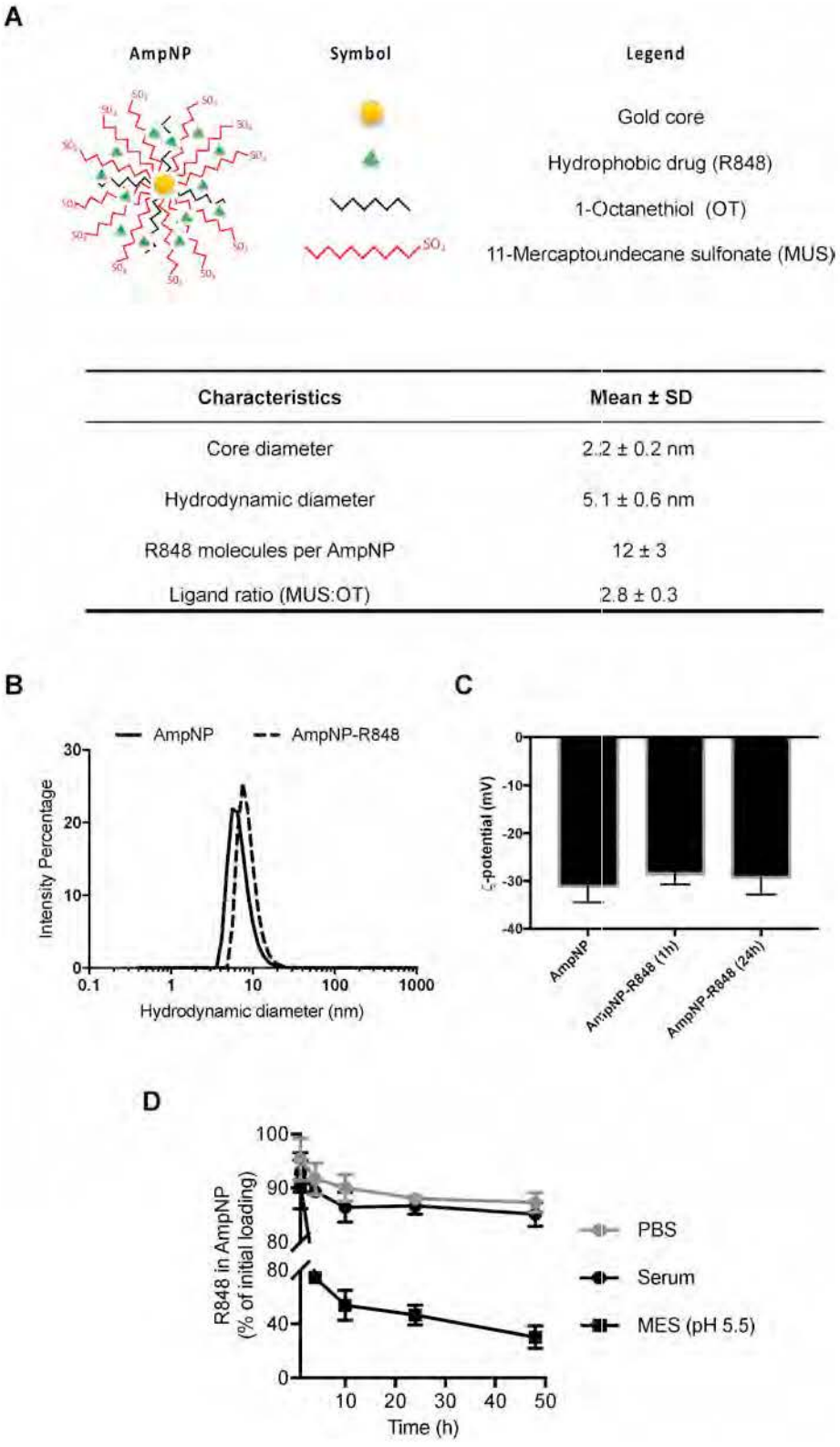

Characteristics	Mean ± SD
Core diameter	2.2 ± 0.2 nm
Hydrodynamic diameter	5.1 ± 0.6 nm
R848 molecules per AmpNP	12 ± 3
Ligand ratio (MUS:OT)	2.8 ± 0.3

Fig. 1. R848 was efficiently loaded onto AmpNP. (A) Illustrative scheme and characteristics of AmpNP. Mean ± SD between 3 different batches synthetized on different days are shown. (B) Hydrodynamic diameter distribution determined by dynamic light scattering and (C) surface zeta-potential measured by Malvern Zetasizer® before and after R848 conjugation. (D) Release kinetics of R848 loaded on AmpNP in PBS, 100% serum and acidic buffer conditions. Graphs represent the mean ± SD of 3 independent experiments.

nodes (inguinal and axillary nodes) with only traces of gold in contralateral lymph nodes (Fig. 2B). Only traces of gold ions were detected in the spleen, reflecting the low levels of particles that reach the systemic circulation. Traces of gold ions were also detected in the liver after subcutaneous injection, whereas none were detected in the lung, kidney, bladder and blood (Supplementary Fig. 4). In contrast, after intravenous injection low levels of gold ions were measured in the spleen and liver (Supplementary Fig. 4).

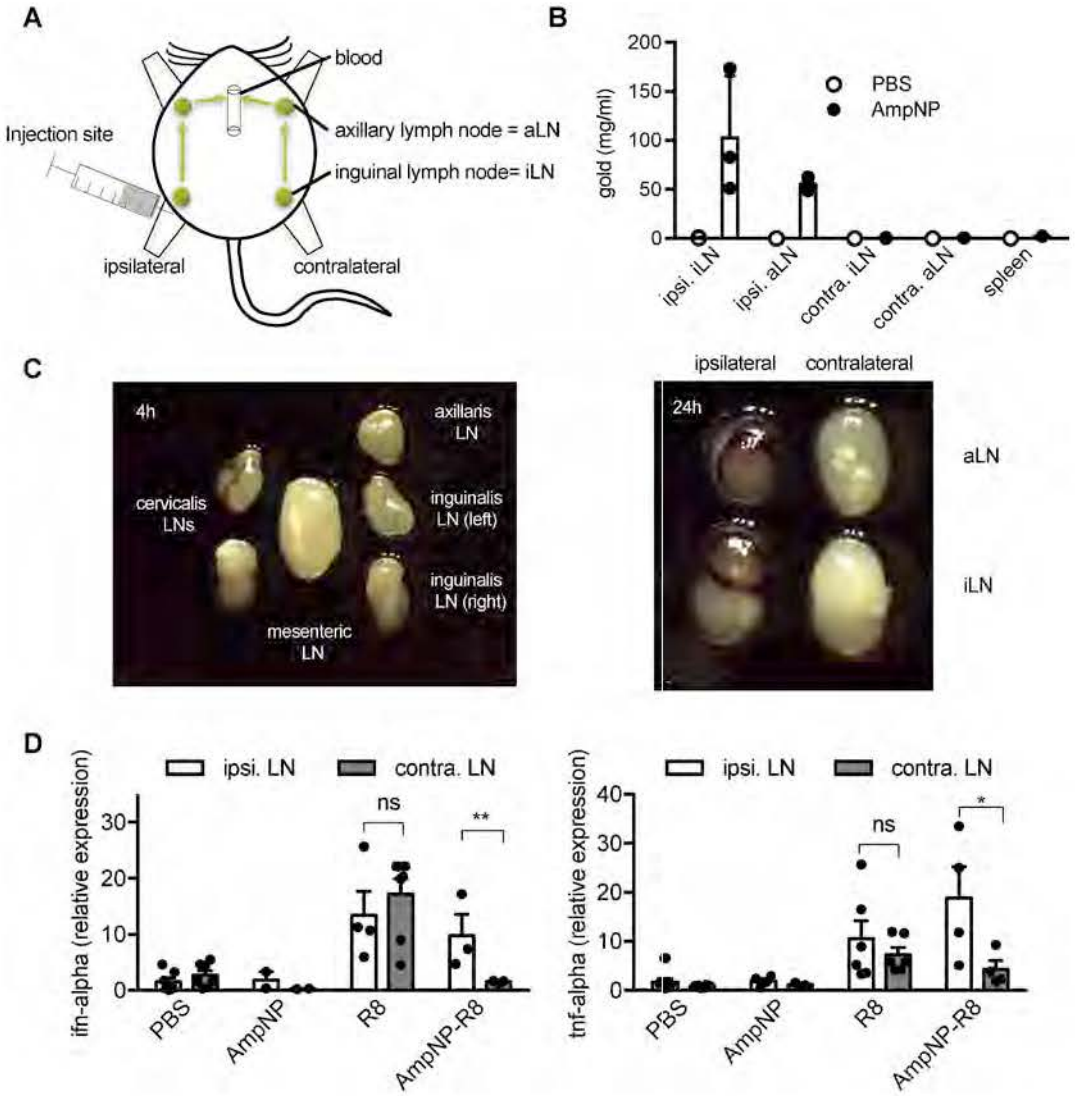

Fig. 2. AmpNP-R848 induced a local immune activation in lymph nodes. Mice were injected s.c. in the inguinal area with 110 µg AmpNP-R8 (total R848 dose 6 µg), an equivalent dose of free R848 (R8) or unloaded AmpNP (AmpNP). (A) Scheme of injection site. (B) Quantification of the gold content by ICP-MS in solubilized lymph nodes 24 h post injection. (C) Stereomicroscopy pictures of the lymph nodes isolated 4 h and 24 h post injection of AmpNP-R8 (representative images of 3 independent experiments). (D) Expression of R848-induced cytokines in lymph nodes 30 min post injection. Results were obtained from at least 3 independent experiments. Each dot represents one mouse. Bars represent the mean ± SD of the pooled data. Asterisks indicate significant difference using unpaired two-tailed Student's T-test. ns: not significant.

Nanoparticles are transported to lymph nodes by two distinct pathways: they can drain with interstitial flow via the lymph or they can be taken up and carried to the lymph node by migratory dendritic cells [5,36]. Due to the relatively small size of AmpNP, which have a mean diameter below 10 nm, it is probable that the AmpNP accumulate passively in the lymph node. Indeed, AmpNP-R848 were detectable in the lymph nodes already 30 min after injection (data not shown). Since the migration of dendritic cells into the lymph node takes approximately 18 h, it is thus unlikely that AmpNP were delivered by dendritic cells [36]. This is in contrast to a previous publication by the authors where polymer-based nanoparticles were used to deliver R848 to the lymph nodes [37]. The larger size of those particles (> 150 nm) probably precluded their passive delivery to the lymph nodes by the lymph and required uptake by migratory dendritic cells.

R848 is known to induce two intracellular pathways of immune activation: (i) the interferon (IFN) pathway controlling the production of IFN-α and (ii) the NF-κB pathway controlling the production of proinflammatory molecules such as TNFα [38]. To assess whether the R848 cargo of AmpNP could fulfill its immunostimulatory function in the lymph nodes, we measured the R848-induced cytokine expression in ipsilateral and contralateral lymph nodes. As expected, free R848 induced expression of IFN-α and TNFα in both ipsilateral and contralateral lymph nodes. In contrast, the equivalent amount of R848 delivered by AmpNP rapidly and efficiently induced ipsilateral expression of both these cytokines, but only low levels of these cytokine transcripts in contralateral lymph nodes (Fig. 2D). AmpNP without cargo did not lead to cytokine expression. Thus, the induction of cytokine expression correlates with the biodistribution of AmpNP in lymphoid organs.

3.4. Antitumor efficacy of AmpNP-R848 in mice

To examine the therapeutic impact of AmpNP delivery of R848, we compared the antitumor efficacy of AmpNP-R848 with free R848. Mice bearing large established CT26 subcutaneous tumors (mean tumor volume of 200 mm^3) were treated subcutaneously with AmpNP-R8 containing 6 µg of R848 or the equivalent dose of free R848 five times at 3-day intervals (Fig. 3A). As expected, free R848 inhibited tumor growth (Fig. 3B). However, the treatment of AmpNP-R848 was more effective than free R848 to inhibit tumor growth (Fig. 3B) and led to an increase

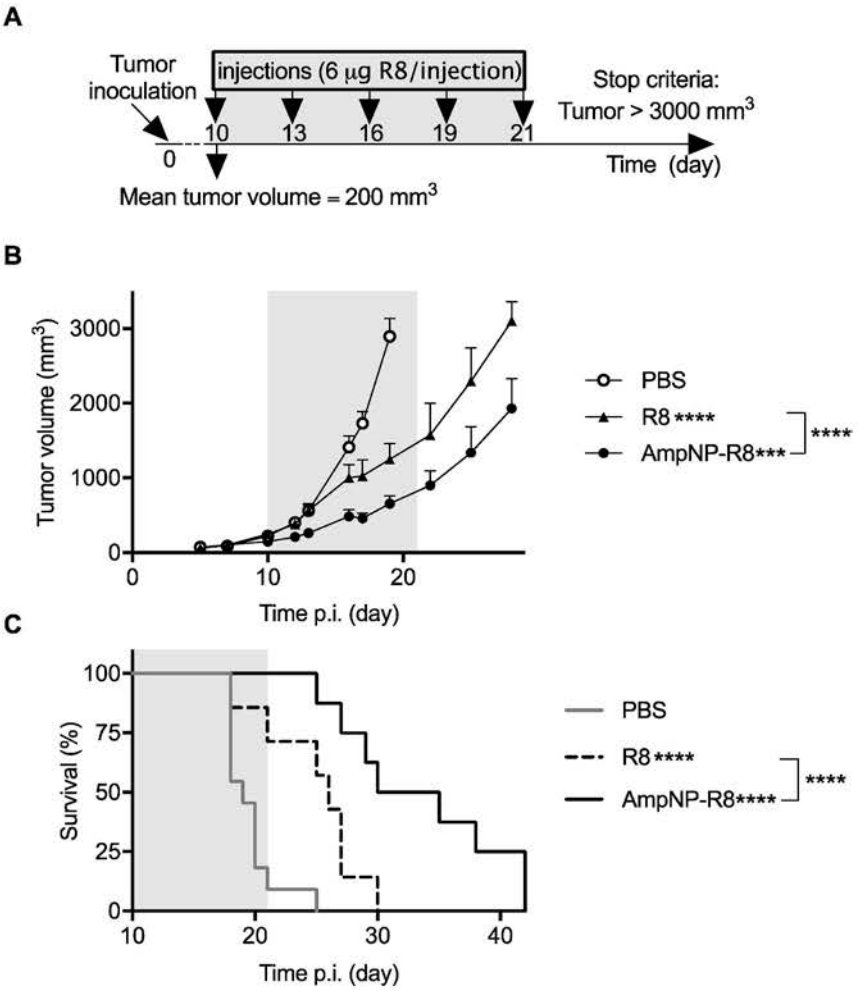

Fig. 3. AmpNP delivery enhanced the antitumor efficacy of R848. (A) CT26 tumor-bearing mice with a tumor volume of 200 mm^3 were injected 5 times at 3-day intervals s.c. in the inguinal area with AmpNP-R8 (R848 dose 6 μg) or an equivalent dose of free R848. (B) Mean tumor volume per treatment group ($n \geq 7$) ± SD. Asterisks indicate significant differences using repeated-measured two-way ANOVA followed by Dunnett's multiple comparison test on day 18. (C) Survival curve. Asterisks indicate significant difference using log-rank test. One representative experiment from 2 independent experiments is shown.

in survival (Fig. 3C). No signs of impaired well-being nor changes in body or spleen weight compared to the control group were observed for the duration of the experiment, supporting the absence of nanoparticle-associated toxicity (Supplementary Fig. 5). Thus, AmpNP delivery enhances the therapeutic effect of R848, even when the treatment is initiated after the establishment of large tumors.

3.5. Impact of AmpNP-R848 on the antitumor immune response

In order to investigate the mechanisms leading to stronger antitumor responses with AmpNP-R848, we assessed whether AmpNP-delivered R848 induced a Th1-type immune response, since this is linked to effective antitumor immunity. A panel of serum cytokines was measured by bead-based immunoassay. Indeed, serum cytokines indicative of a Th1 response, such as IL-12 and IFN-γ, were increased after AmpNP-R848 treatment (Supplementary Fig. 6). In addition, other pro-inflammatory cytokines and chemokines were induced (IL-6, GM-CSF and CCL2). Generally, however, no significant difference in serum cytokine levels was seen when compared to treatment with the same amount of free R848 at the time points examined. The other cytokines tested by the immunoassay (IL-1α, IL-1β, IL-23, IL-10, IL-27 and IL-17A) were not detected in the serum of treated mice (data not shown). Altogether, this demonstrated that R848 delivered by AmpNP induced a systemic Th1 cytokine response similar to the one induced by free R848. In addition, some types of nanoparticles activate the inflammasome machinery within immune cells and thus have an intrinsic proinflammatory activity which can be deleterious [39,40]. As neither unloaded AmpNP nor AmpNP-R848 induced secretion of the inflammasome-dependent IL-1α and IL-1β, it is probable that these particles do not activate the inflammasome.

The main effectors of antitumor immunity are cytotoxic T cells, which are known to directly kill tumor cells. These cytotoxic cells, which need to be specific for tumor antigens, are generated in the tumor-draining lymph nodes and can then migrate to other lymphoid organs such as the spleen [41,42]. We assessed the number of splenic cytotoxic T cells that specifically recognized the immunodominant CT26 tumor antigen gp70 in tumor-bearing mice treated by AmpNP-R848, using a well-described MHC-tetramer assay [43]. R848 delivered by AmpNP generated tumor-specific cytotoxic T cells more efficiently than the equivalent dose of free R848 (Fig. 4A). Additionally, the cytotoxic T cells exhibited higher levels of the activation markers PD1 and CD69 on their surface (Fig. 4B). Thus, the improved antitumor efficacy of AmpNP-R848 compared to free R848 was associated with higher numbers and higher activation levels of tumor-specific cytotoxic T cells.

4. Discussion and conclusions

In summary, we have developed highly stable gold nanoparticles that home to the lymph nodes for efficient immunotherapeutic delivery and whose densely packed amphiphilic ligand shell can be easily loaded

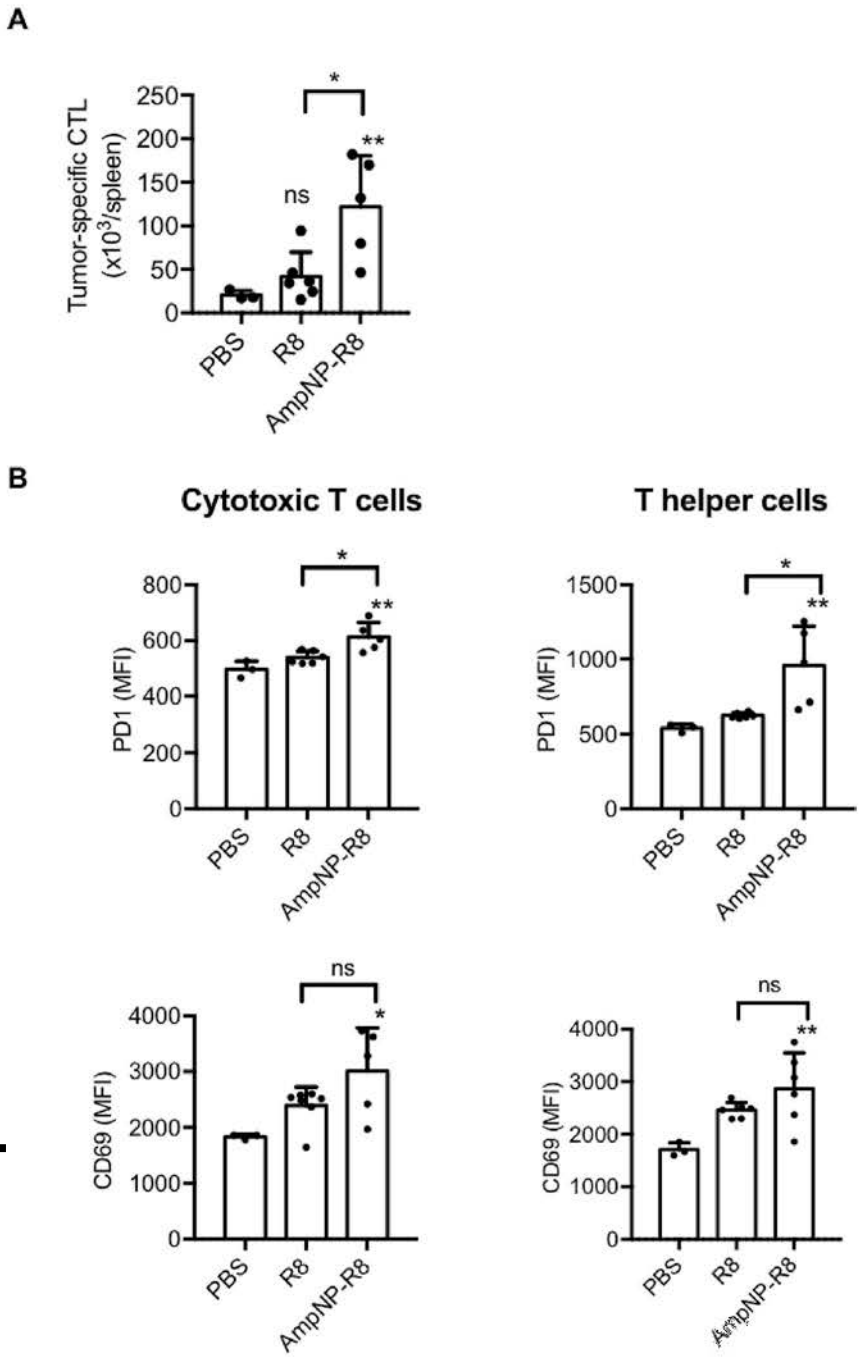

Fig. 4. AmpNP-R848 induced activated, tumor-specific cytotoxic T cells in tumor-bearing mice. CT26 tumor-bearing mice were treated with AmpNP-R8 or R848 as in Fig. 3. T-cell responses were measured in the spleen one day after the last injection. (A) Number of tumor-specific cytotoxic T cells (CTL) per spleen. (B) Activation markers on the surface of cytotoxic T cells and T helper cells. Each dot represents one mouse. Bars represent the mean ± SD. Asterisks without brackets indicate significant difference to the untreated group using one-way ANOVA followed by Dunnett's multiple comparison test. Asterisks with brackets indicates significant difference using unpaired two-tailed Student's T-test. ns: not significant.

with the unmodified immunostimulant drug R848. The particle delivery clearly improved the antitumor effect of the drug and enhanced survival in mice with large established tumors. The approach for R848 accommodation on AmpNP did not involve any complex covalent conjugation process while preserving stability. In addition, the subcutaneous application route promoted the direct transport of the particles to the lymph nodes, which are the site of action of the drug, without accumulation in the spleen, which suggests absence of the particles in the circulation. The drawbacks associated with intravenous injection, including accumulation of nanoparticles in highly perfused organs such as the spleen and the liver or the rapid clearance of nanoparticles by the kidney, may therefore be avoided.

Despite a localized application, a systemic antitumor response was induced, as seen by the presence of tumor-specific T cells in the spleen following AmpNP-R848 treatment. Such a systemic immune response is necessary to detect and eliminate metastases at distant sites [44]. Importantly, this strategy of targeting the lymph nodes took advantage of endogenous tumor antigens, which are transported to the lymph nodes draining the tumor by dendritic cells [45]. Thus, tumor-specific T cells were activated without the need to apply exogenous antigen, and the delivery strategy therefore bypassed the requirement to identify individual tumor antigens for each patient. This is in contrast to previously published nanoparticle-based TLR7 agonist delivery for cancer therapy, which was done in co-administration with tumor antigens [46–48].

The antitumor efficacy of AmpNP-R848 may be enhanced by combination with recently developed treatments targeting immune checkpoint, such as anti-PD-1 antibodies. Indeed, our results showed that R848 delivered by AmpNP increased the expression of the immune checkpoint molecules PD1 on T cells. The combination of a therapeutic antibody blocking this immune checkpoint with AmpNP-R848 delivery may thus further improve the efficacy of the treatment. Overall, the

highly stable amphiphilic nature of gold nanoparticles makes them promising candidates for delivery of TLR7 agonists to the lymph node in the context of cancer immunotherapy.

Conflict of interest

The authors declare no financial conflicts of interest.

Data availability

The raw/processed data required to reproduce these findings cannot be shared at this time due to legal reasons.

Acknowledgments

This study was supported by the National Center of Competence in Research (NCCR) for Bio-Inspired Materials and the Swiss National Science Foundation grants 310030_156871 and 310030_156372, as well as the Melanoma Research Alliance. The authors thank A. Oberson and J. Widmer for technical support.

Appendix A. Supplementary data

Supplementary data to this article can be found online

References

[1] J. Larkin, V. Chiarion-Sileni, R. Gonzalez, J.J. Grob, C.L. Cowey, C.D. Lao, D. Schadendorf, R. Dummer, M. Smylie, P. Rutkowski, P.F. Ferrucci, A. Hill, J. Wagstaff, M.S. Carlino, J.B. Haanen, M. Maio, I. Marquez-Rodas, G.A. McArthur, P.A. Ascierto, G.V. Long, M.K. Callahan, M.A. Postow, K. Grossmann, M. Sznol, B. Dreno, L. Bastholt, A. Yang, L.M. Rollin, C. Horak, F.S. Hodi, J.D. Wolchok, Combined nivolumab and ipilimumab or monotherapy in untreated melanoma, N. Engl. J. Med. 373 (2015) 23–34, https://doi.org/10.1056/NEJMoa1504030.

[2] G.J. Randolph, V. Angeli, M.A. Swartz, Dendritic-cell trafficking to lymph nodes through lymphatic vessels, Nat. Rev. Immunol. 5 (2005) 617–628, https://doi.org/10.1038/nri1670.

[3] P. Johansen, A.C. Häffner, F. Koch, K. Zepter, I. Erdmann, K. Maloy, J.J. Simard, T. Storni, G. Senti, A. Bot, B. Wüthrich, T.M. Kündig, Direct intralymphatic injection of peptide vaccines enhances immunogenicity, Eur. J. Immunol. 35 (2005) 568–574, https://doi.org/10.1002/eji.200425599.

[4] K.J. Maloy, I. Erdmann, V. Basch, S. Sierro, T. a Kramps, R.M. Zinkernagel, S. Oehen, T.M. Kündig, Intralymphatic immunization enhances DNA vaccination, Proc. Natl. Acad. Sci. U. S. A 98 (2001) 3299–3303, https://doi.org/10.1073/pnas.051630798.

[5] D.J. Irvine, M.A. Swartz, G.L. Szeto, Engineering synthetic vaccines using cues from natural immunity, Nat. Mater. 12 (2013) 978–990, https://doi.org/10.1038/nmat3775.

[6] T. Storni, T.M. Kündig, G. Senti, P. Johansen, Immunity in response to particulate antigen-delivery systems, Adv. Drug Deliv. Rev. 57 (2005) 333–355, https://doi.org/10.1016/j.addr.2004.09.008.

[7] K. Palucka, J. Banchereau, Cancer immunotherapy via dendritic cells, Nat. Rev. Canc. 12 (2012) 265–277, https://doi.org/10.1038/nrc3258.

[8] K. Shao, S. Singha, X. Clemente-Casares, S. Tsai, Y. Yang, P. Santamaria, Nanoparticle-based immunotherapy for cancer, ACS Nano 9 (2015) 16–30, https://doi.org/10.1021/nn5062029.

[9] J. Conniot, J.M. Silva, J.G. Fernandes, L.C. Silva, R. Gaspar, S. Brocchini, H.F. Florindo, T.S. Barata, Cancer immunotherapy: nanodelivery approaches for immune cell targeting and tracking, Front. Chem. 2 (2014) 105, https://doi.org/10.3389/fchem.2014.00105.

[10] S. Wilhelm, A.J. Tavares, Q. Dai, S. Ohta, J. Audet, H.F. Dvorak, W.C.W. Chan, Analysis of nanoparticle delivery to tumours, Nat. Rev. Mater. 1 (2016), https://doi.org/10.1038/natrevmats.2016.14.

[11] D.J. Irvine, Y.S.Y. Yang, A. Bekdemir, F. Stellacci, Nanoparticles Comprising a Metal Core Surrounded by a Monolayer for Lymph Node Targeting, WO2017070676A1 (2017).

[12] Y.S.S. Yang, P.U. Atukorale, K.D. Moynihan, A. Bekdemir, K. Rakhra, L. Tang, F. Stellacci, D.J. Irvine, High-throughput quantitation of inorganic nanoparticle biodistribution at the single-cell level using mass cytometry, Nat. Commun. 8 (2017), https://doi.org/10.1038/ncomms14069.

[13] C.K. Kim, P. Ghosh, C. Pagliuca, Z.J. Zhu, S. Menichetti, V.M. Rotello, Entrapment of hydrophobic drugs in nanoparticle monolayers with efficient release into cancer cells, J. Am. Chem. Soc. 131 (2009) 1360–1361, https://doi.org/10.1021/ja808137c.

[14] T.L. Wagner, C.L. Ahonen, A.M. Couture, S.J. Gibson, R.L. Miller, R.M. Smith, M.J. Reiter, J.P. Vasilakos, M.A. Tomai, Modulation of TH1 and TH2 cytokine production with the immune response modifiers, R-848 and imiquimod, Cell. Immunol. 191 (1999) 10–19, https://doi.org/10.1006/cimm.1998.1406.

[15] E. Stockfleth, U. Trefzer, C. Garcia-Bartels, T. Wegner, T. Schmook, W. Sterry, The use of Toll-like receptor-7 agonist in the treatment of basal cell carcinoma: an overview, Br. J. Dermatol. 149 (Suppl) (2003) 53–56 doi:5626 [pii].

[16] C. Bourquin, C. Hotz, D. Noerenberg, A. Voelkl, S. Heidegger, L.C. Roetzer, B. Storch, N. Sandholzer, C. Wurzenberger, D. Anz, S. Endres, Systemic cancer therapy with a small molecule agonist of toll-like receptor 7 can be improved by circumventing TLR tolerance, Cancer Res. 71 (2011) 5123–5133, https://doi.org/10.1158/0008-5472.CAN-10-3903.

[17] T. Spinetti, L. Spagnuolo, I. Mottas, C. Secondini, M. Treinies, C. Rüegg, C. Hotz, C. Bourquin, TLR7-based cancer immunotherapy decreases intratumoral myeloid-derived suppressor cells and blocks their immunosuppressive function, Oncoimmunology 5 (2016), https://doi.org/10.1080/2162402X.2016.1230578.

[18] D. Goldstein, P. Hertzog, E. Tomkinson, D. Couldwell, S. McCarville, S. Parrish, P. Cunningham, M. Newell, M. Owens, D.A. Cooper, Administration of imiquimod, an interferon inducer, in asymptomatic human immunodeficiency virus-infected persons to determine safety and biologic response modification, J. Infect. Dis. 178 (1998) 858–861, https://doi.org/10.1086/515343.

[19] P.J. Pockros, D. Guyader, H. Patton, M.J. Tong, T. Wright, J.G. McHutchison, T.C. Meng, Oral resiquimod in chronic HCV infection: safety and efficacy in 2 placebo-controlled, double-blind phase IIa studies, J. Hepatol. 47 (2007) 174–182, https://doi.org/10.1016/j.jhep.2007.02.025.

[20] V. Cagno, P. Andreozzi, M. D'Alicarnasso, P.J. Silva, M. Mueller, M. Galloux, R. Le Goffic, S.T. Jones, M. Vallino, J. Hodek, J. Weber, S. Sen, E.R. Janecek, A. Bekdemir, B. Sanavio, C. Martinelli, M. Donalisio, M.A.R. Welti, J.F. Eleouet, Y. Han, L. Kaiser, L. Vukovic, C. Tapparel, P. Král, S. Krol, D. Lembo, F. Stellacci, Broad-spectrum non-toxic antiviral nanoparticles with a virucidal inhibition mechanism, Nat. Mater. 17 (2018) 195–203, https://doi.org/10.1038/NMAT5053.

[21] A. Bekdemir, F. Stellacci, A centrifugation-based physicochemical characterization method for the interaction between proteins and nanoparticles, Nat. Commun. 7 (2016), https://doi.org/10.1038/ncomms13121.

[22] P. Andreozzi, C. Martinelli, R.P. Carney, T.M. Carney, F. Stellacci, Erythrocyte incubation as a method for free-dye presence determination in fluorescently labeled nanoparticles, Mol. Pharm. 10 (2013) 875–882, https://doi.org/10.1021/mp300530c.

[23] J. Helft, J. Böttcher, P. Chakravarty, S. Zelenay, J. Huotari, B.U. Schraml, D. Goubau, C. Reis e Sousa, GM-CSF mouse bone marrow cultures comprise a heterogeneous population of CD11c^{+}MHCII^{+} macrophages and dendritic cells, Immunity 42 (2015) 1197–1211, https://doi.org/10.1016/j.immuni.2015.05.018.

[24] I. Mottas, A. Milosevic, A. Petri-Fink, B. Rothen-Rutishauser, C. Bourquin, A rapid screening method to evaluate the impact of nanoparticles on macrophages, Nanoscale 9 (2017) 2492–2504, https://doi.org/10.1039/c6nr08194k.

[25] K. Ulbrich, K. Holá, V. Šubr, A. Bakandritsos, J. Tuček, R. Zbořil, Targeted drug delivery with polymers and magnetic nanoparticles: covalent and noncovalent approaches, release control, and clinical studies, Chem. Rev. 116 (2016) 5338–5431, https://doi.org/10.1021/acs.chemrev.5b00589.

[26] L. Wu, J. Zhang, W. Watanabe, Physical and chemical stability of drug nanoparticles, Adv. Drug Deliv. Rev. 63 (2011) 456–469, https://doi.org/10.1016/j.addr.2011.02.001.

[27] V. Amendola, R. Pilot, M. Frasconi, O.M. Maragò, M.A. Iatì, Surface plasmon resonance in gold nanoparticles: a review, J. Phys. Condens. Matter 29 (2017) 203002, , https://doi.org/10.1088/1361-648X/aa60f3.

[28] T.L. Moore, L. Rodriguez-Lorenzo, V. Hirsch, S. Balog, D. Urban, C. Jud, B. Rothen-Rutishauser, M. Lattuada, A. Petri-Fink, Nanoparticle colloidal stability in cell culture media and impact on cellular interactions, Chem. Soc. Rev. 44 (2015) 6287–6305, https://doi.org/10.1039/c4cs00487f.

[29] R.H. Fang, L. Zhang, Nanoparticle-based modulation of the immune system, Annu. Rev. Chem. Biomol. Eng. 7 (2016) 305–326, https://doi.org/10.1146/annurev-chembioeng-080615-034446.

[30] H. Hemmi, T. Kaisho, O. Takeuchi, S. Sato, H. Sanjo, K. Hoshino, T. Horiuchi, H. Tomizawa, K. Takeda, S. Akira, Small-antiviral compounds activate immune cells via the TLR7 MyD88-dependent signaling pathway, Nat. Immunol. 3 (2002) 196–200, https://doi.org/10.1038/ni758.

[31] S.J. Gibson, J.M. Lindh, T.R. Riter, R.M. Gleason, L.M. Rogers, A.E. Fuller, J.A.L. Oesterich, K.B. Gorden, X. Qiu, S.W. McKane, R.J. Noelle, R.L. Miller, R.M. Kedl, P. Fitzgerald-Bocarsly, M.A. Tomai, J.P. Vasilakos, Plasmacytoid dendritic cells produce cytokines and mature in response to the TLR7 agonists, imiquimod and resiquimod, Cell. Immunol. 218 (2002) 74–86, https://doi.org/10.1016/S0008-8749(02)00517-8.

[32] C. Hotz, C. Bourquin, Systemic cancer immunotherapy with Toll-like receptor 7 agonists: timing is everything, Oncoimmunology 1 (2012) 227–228, https://doi.org/10.4161/onci.1.2.18169.

[33] E. Orsini, A. Guarini, S. Chiaretti, F.R. Mauro, R. Foa, The circulating dendritic cell compartment in patients with chronic lymphocytic leukemia is severely defective and unable to stimulate an effective T-cell response, Cancer Res. 63 (2003) 4497–4506, https://doi.org/10.1038/32588.

[34] A. Grakoui, S.K. Bromley, C. Sumen, M.M. Davis, A.S. Shaw, P.M. Allen, M.L. Dustin, The immunological synapse: a molecular machine controlling T cell activation, Science 285 (80) (1999) 221–227, https://doi.org/10.1126/science.285.5425.221.

[35] N.L. Tilney, Patterns of lymphatic drainage in the adult laboratory rat, J. Anat. 109 (1971) 369–383.

[36] V. Manolova, A. Flace, M. Bauer, K. Schwarz, P. Saudan, M.F. Bachmann, Nanoparticles target distinct dendritic cell populations according to their size, Eur. J. Immunol. 38 (2008) 1404–1413, https://doi.org/10.1002/eji.200737984.

[37] J. Widmer, C. Thauvin, I. Mottas, V.N. Nguyen, F. Delie, E. Allémann, C. Bourquin, Polymer-based nanoparticles loaded with a TLR7 ligand to target the lymph node for immunostimulation, Int. J. Pharm. 535 (2018) 444–451, https://doi.org/10.1016/j.ijpharm.2017.11.031.
[38] C. Maisonneuve, S. Bertholet, D.J. Philpott, E. De Gregorio, Unleashing the potential of NOD- and Toll-like agonists as vaccine adjuvants, Proc. Natl. Acad. Sci. 111 (2014) 12294–12299, https://doi.org/10.1073/pnas.1400478111.
[39] S.L. Demento, S.C. Eisenbarth, H.G. Foellmer, C. Platt, M.J. Caplan, W. Mark Saltzman, I. Mellman, M. Ledizet, E. Fikrig, R.A. Flavell, T.M. Fahmy, Inflammasome-activating nanoparticles as modular systems for optimizing vaccine efficacy, Vaccine 27 (2009) 3013–3021, https://doi.org/10.1016/j.vaccine.2009.03.034.
[40] F. Martinon, V. Pétrilli, A. Mayor, A. Tardivel, J. Tschopp, Gout-associated uric acid crystals activate the NALP3 inflammasome, Nature 440 (2006) 237–241, https://doi.org/10.1038/nature04516.
[41] M.F. Krummel, F. Bartumeus, A. Gérard, T cell migration, search strategies and mechanisms, Nat. Rev. Immunol. 16 (2016) 193–201, https://doi.org/10.1038/nri.2015.16.
[42] D. Finlay, D.A. Cantrell, Metabolism, migration and memory in cytotoxic T cells, Nat. Rev. Immunol. 11 (2011) 109–117, https://doi.org/10.1038/nri2888.
[43] C. Hotz, M. Treinies, I. Mottas, L.C. Rötzer, A. Oberson, L. Spagnuolo, M. Perdicchio, T. Spinetti, T. Herbst, C. Bourquin, Reprogramming of TLR7 signaling enhances antitumor NK and cytotoxic T cell responses, Oncoimmunology 5 (2016), https://doi.org/10.1080/2162402X.2016.1232219.
[44] A. Ribas, R. Dummer, I. Puzanov, A. VanderWalde, R.H.I. Andtbacka, O. Michielin, A.J. Olszanski, J. Malvehy, J. Cebon, E. Fernandez, J.M. Kirkwood, T.F. Gajewski, L. Chen, K.S. Gorski, A.A. Anderson, S.J. Diede, M.E. Lassman, J. Gansert, F.S. Hodi, G.V. Long, Oncolytic virotherapy promotes intratumoral T cell infiltration and improves anti-PD-1 immunotherapy, Cell 170 (2017), https://doi.org/10.1016/j.cell.2017.08.027 1109–1119.e10.
[45] E.W. Roberts, M.L. Broz, M. Binnewies, M.B. Headley, A.E. Nelson, D.M. Wolf, T. Kaisho, D. Bogunovic, N. Bhardwaj, M.F. Krummel, Critical role for CD103+/CD141+ Dendritic cells bearing CCR7 for tumor antigen trafficking and priming of T cell immunity in melanoma, Cancer Cell 30 (2016) 324–336, https://doi.org/10.1016/j.ccell.2016.06.003.
[46] L.M. Kranz, M. Diken, H. Haas, S. Kreiter, C. Loquai, K.C. Reuter, M. Meng, D. Fritz, F. Vascotto, H. Hefesha, C. Grunwitz, M. Vormehr, Y. Hüsemann, A. Selmi, A.N. Kuhn, J. Buck, E. Derhovanessian, R. Rae, S. Attig, J. Diekmann, R.A. Jabulowsky, S. Heesch, J. Hassel, P. Langguth, S. Grabbe, C. Huber, Ö. Türeci, U. Sahin, Systemic RNA delivery to dendritic cells exploits antiviral defence for cancer immunotherapy, Nature 534 (2016) 396–401, https://doi.org/10.1038/nature18300.
[47] M.B. Heo, Y.T. Lim, Programmed nanoparticles for combined immunomodulation, antigen presentation and tracking of immunotherapeutic cells, Biomaterials 35 (2014) 590–600, https://doi.org/10.1016/j.biomaterials.2013.10.009.
[48] C. Bourquin, C. Wurzenberger, S. Heidegger, S. Fuchs, D. Anz, S. Weigel, N. Sandholzer, G. Winter, C. Coester, S. Endres, Delivery of immunostimulatory RNA oligonucleotides by gelatin nanoparticles triggers an efficient antitumoral response, J. Immunother. 33 (2010) 935–944, https://doi.org/10.1097/CJI.0b013e3181f5dfa7.